Photogrammetry from Aircraft Side Camera Movies: Winter MONEX

CHARLES WARNER

Department of Environmental Science, University of Virginia, Charlottesville 22903

(Manuscript received 24 March 1981, in final form 12 August 1981)

ABSTRACT

A new method is described for photogrammetry of clouds from aircraft side camera movies, to take into account cloud motion. In extreme circumstances of measurement, this leads to improvements of 500 m in cloud height. General use of the method is desirable when cloud measurements are related to other data.

On 10 December 1978 over the South China Sea, cumulus fractus were of depth ~0.2 km, and updrafts were of width ~0.25 km. For humilis the corresponding numbers were 0.7 and 0.4 km. Mediocris with tops at height (z) 2.2 km had updrafts of width (w) ~1.3 km. Updrafts in congestus towers increased with height, with dw/dz ~0.17, a figure similar to that found for day 245 of the GARP Atlantic Tropical Experiment.

Cloud number densities on 10 December varied over an order of magnitude over distances of 100 km, even in circumstances relatively uniform on the large scale. Order of magnitude estimates of percent area coverage by updrafts yield values up to 10% for fractus and humilis combined, up to a few percent for mediocris, and less than 1% for congestus in the mid-troposphere. An area measuring 1° latitude × 2° longitude was found to contain nine cumulonimbi, yielding ≈0.1% coverage by updrafts in the mid-troposphere.

1. Introduction

Positions of clouds have been measured, using time-lapse movies taken from aircraft, to describe cloud patterns in synoptic context, and for purposes of comparison with satellite determinations. A new method of photogrammetry is described in this paper, following previous experience in this work (Warner, 1978; Warner *et al.*, 1979).

For an aircraft flying steadily past a cloud with a side-pointing cine-camera of constant frame rate, the range of the cloud is nearly proportional to the time, or the number of frames of film, required for it to pass across the field of view. If the position of the aircraft is known for any arbitrarily chosen frame, then the cloud position may be plotted on a plan view map. The height of the cloud may be found by measuring its elevation relative to the horizon, and coupling this with the range. Practical experience with a simple technique along these lines, adapted to computers, indicated accuracies of cloud heights of ~500 m. The accuracy is much greater for clouds near the aircraft than for those at great distances.

During the winter monsoon experiment WMONEX (Greenfield and Krishnamurti, 1979) the NOAA WP3D and NCAR Electra aircraft flew dropwindsonde missions at altitude 6–8 km over the South China Sea. Side camera movies are available for measuring cloud positions. It is desirable to be able to measure heights of cumulus fractus based ~500 m above the surface, moving at speeds near 20 m s^{-1} in the strong low-level northeasterly monsoon current. This velocity was about one fifth of that of the aircraft, and was parallel to the aircraft motion, a situation unfavorable for accurate photogrammetry without taking the cloud translation into account, because of introduction of an error of one fifth in the photogrammetric baseline. The range, and thence the height of the cloud, follow directly from the length of the baseline. Another difficulty was that the Electra performed a pronounced oscillation about straight and level flight, most noticeable in terms of changes of heading and roll angle. A new computation designed to cope with those problems is described below. The gain in accuracy, relative to the previous technique, is several hundred meters for heights of such clouds as the WMONEX cumulus fractus.

After describing the measurement of cloud heights and horizontal positions in Sections 2 to 4, and presenting individual clouds in Section 5, a method for measuring cloud number densities and fractional area coverage is described in Section 6. Then follow cloud population data for 10 December 1978 over the South China Sea, a situation treated by Houze *et al.* (1981), Johnson and Priegnitz (1981), and in papers presented at the International Conference on Early Results of FGGE and Large-Scale Aspects of the Monsoon Experiment, in Tallahassee in January 1981.

0021-8952/81/121516-11$06.75

2. Initial data

Before beginning photogrammetry, the following data are assembled: (i) Aircraft position (latitude, longitude, altitude), heading, roll angle and velocity as a function of time, and (ii) movie frame number as a function of time. The former data (i) are available from the National Center for Atmospheric Research, with 1 s resolution; the latter (ii) were obtained by plotting the roll as a function of time for selected intervals, and comparing this plot with the movie. With rapid changes in roll occurring at turns, a precision of 1 or 2 s is generally obtainable for the time of any chosen frame. (The Electra right-side movies readily showed time in a small illuminated panel.) Also required are the effective focal length of the camera multiplied by the magnification due to projection (the product F), the nadir angle of the principal axis of the camera (N, which had values near 88° for the WP3D, and 90° for the Electra), and the amount by which the camera axis was pointed behind the true normal to the aircraft (ψ, a small angle). The parameters F, N and ψ may be adjusted after measurements of known features (coastlines, the horizon, clouds measured from other aircraft, or clouds positioned from their radar echoes).

The calculation is designed to treat uniform translation of the cloud being measured, so an initial estimate is made of cloud velocity (speed v_c and direction θ from which the cloud is moving). For WMONEX I have used the synoptic analyses by R. H. Simpson and Brian J. Morrison, who have integrated dropwindsonde data for wind as a function of height, Soviet ship rawinsondes, and satellite cloud tracking under F. R. Mosher at the University of Wisconsin. Guidance in estimating cloud velocities comes partly from experience with ground-based time-lapse movies of clouds (Warner *et al.*, 1973). For instance, these allow one to observe growth of cumulus on the upshear side (Malkus, 1952), with gradual acceleration to environmental velocities as buoyancy disappears (Warner, 1972). A young small cumulus moves with a velocity close to that of air below cloud base (Telford and Wagner, 1974)—while it is active. Thereafter as it evaporates it appears to move with the wind at its level. A tower of cumulus congestus follows a complex path dictated by the winds at the levels through which it rises (Warner, 1972). Cirrus plumes appear to drift with the wind, thinning by evaporation fairly uniformly along their length. These guidelines for subjective estimates of cloud velocity are not precise—they probably yield an accuracy near 5 m s^{-1} in most cases. This effect is important for cumulus fractus moving at about 20 m s^{-1}. On 10 December 1978, the WP3D flew first northward toward Hong Kong—a direction opposed to those of the low-level winds. Then it turned around and flew southward, in much the same direction as the low-level winds. Calculations of the base heights of cumulus fractus without incorporating a cloud velocity put them near sea level in the first case and near 1 km in the second. With appropriate cloud velocities, results came close to 500 m. There are independent data which confirm that this figure is roughly correct.

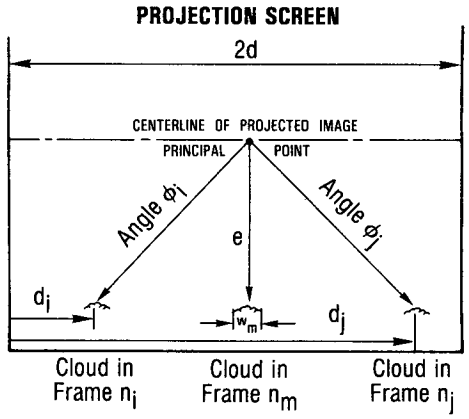

FIG. 1. Projected images from a right-side camera movie. The cloud first appears at left. The frame number n_i and distance d_i on the screen are noted. When the cloud is in the middle of the field of view, the frame number n_m and distances e and w_m are noted. When the cloud is last seen, the frame number n_j and distance d_j are noted. The distance $e > 0$ when the cloud is above the principal point. Here $e < 0$. As the movie is run, the principal point moves up and down with small changes of roll of the aircraft. Thus the elevation measurement e must be coupled with knowledge of the roll of the aircraft at frame n_m. The approximate width w_m of a cumulus is measured a little below the top.

3. Theory

Figures shown below are drawn for the case of a right-side camera, for which an indicator k is set equal to 1. For a left-side camera $k = -1$. From projected images of the movie, seven measurements are made, as shown in Fig. 1: the frame numbers n_i, n_m and n_j, and the distances d_i, e, w_m and d_j. The width w_m of a growing cumulus tower is an assessment of the width of the central rising motion, distinguishable from the periphery of the ring vortex circulation, which subsides (Warner *et al.*, 1973). From tables of frame number against time, and of roll angle against time, the frame number n_m yields the roll r (positive to starboard) corresponding to the elevation measurement e.

Eq. (1) below yields the angle ϕ between the direction of the cloud from the camera, and the reference axis of the camera pointed at nadir angle ($N - kr$). With the help of Fig. 1, it may be seen that

$$F^2 \tan^2\phi_n \sim (d - d_n)^2 + e^2 \quad (n = i \text{ or } j), \quad (1)$$

where $2d$ is the overall width of the projected image. The Appendix gives further details.

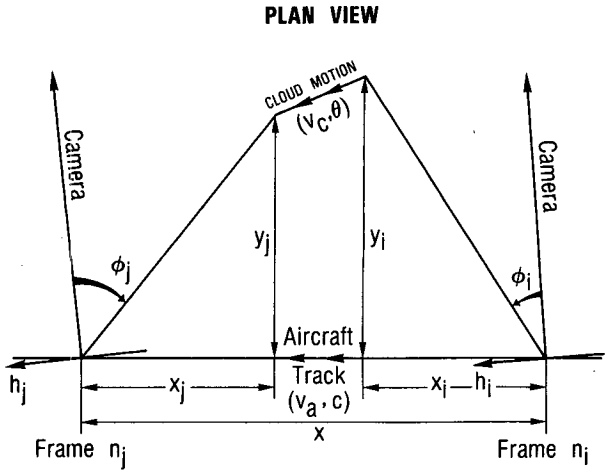

FIG. 2. Plan view of aircraft and cloud motion. At frame n_i the aircraft heading is h_i and the cloud is seen at the diagonal angle ϕ_i (Fig. 1). While the aircraft moves at speed v_a toward the direction c (its track over the ground), the cloud moves at speed v_c from direction θ. Then at frame n_j, with the aircraft heading h_j, the cloud is seen at angle ϕ_j (Fig. 1). More details are shown in Fig. 3.

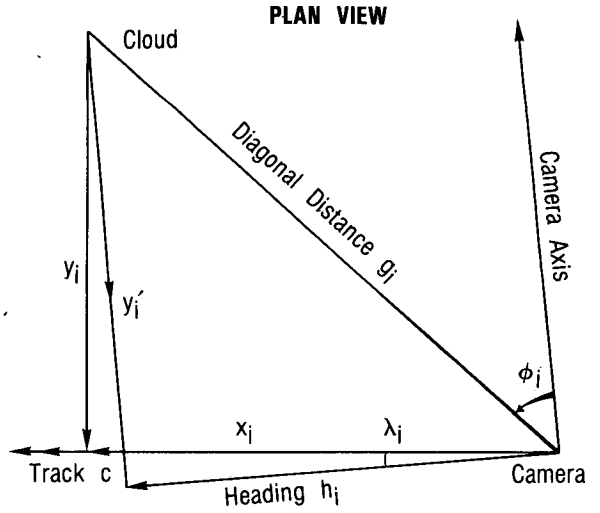

FIG. 3. Plan view of frame n_i. The camera moves along the aircraft track, to which distances x_i and y_i are referred (Fig. 2). The distance y_i' is referred to the vertical plane through the camera axis. The small angle λ_i equals (track-heading-$k\psi$), where ψ is the small angle, nominally zero and not illustrated here, between the vertical plane of the camera axis and that normal to the aircraft heading. (ψ is *positive* if the camera is misaligned toward the *rear* of the aircraft.) The distance g_i separates camera and cloud. The diagonal angle ϕ_i is measured from the camera axis (Fig. 1).

The geometry of measurement in plan view is shown in Fig. 2. Taking into account motion of the aircraft at speed v_a toward direction c, and motion of the cloud at speed v_c from direction θ, plan view distances x and y shown in Fig. 2 are related as follows:

$$x = k(x_i - x_j) - v_c t \cos(c - \theta), \quad (2)$$

$$0.5(y_i - y_j) = -0.5kv_c t \sin(c - \theta). \quad (3)$$

The time t in these equations is the time between frames n_i and n_j. The distances x_n in Eq. (2) have the same signs as the measured quantities $(d - d_n)$ indicated in Fig. 1 (unless the cloud lies between the vertical plane normal to the track and that which includes the camera axis—an unusual case).

For purposes of calculating cloud height, the range $\bar{y}$ is taken as the mean of y_i and y_j. Then from Eq. (3),

$$y_i = \bar{y} - 0.5kv_c t \sin(c - \theta), \quad (4)$$

$$y_j = \bar{y} + 0.5kv_c t \sin(c - \theta), \quad (5)$$

It is necessary to obtain equations relating the distances x and y in Fig. 2 to the measured angles ϕ and h. As shown in Fig. 3, x and y must be referred to a reference axis defined by a small drift angle λ:

$$\lambda_n = c - (h_n + k\psi) \quad (n = i \text{ or } j). \quad (6)$$

Then the distance y_n' in Fig. 3 is given by

$$y_n' = y_n \cos\lambda_n + x_n \sin\lambda_n \quad (n = i \text{ or } j). \quad (7)$$

A further equation for y_n' is obtained from considering a vertical plane normal to the aircraft heading (Fig. 4). It is satisfactory to assume that the height of the cloud does not change appreciably during the measurement, and that a vertical separation z exists between the cloud and the aircraft. Then the diagonal distance g_n is given by

$$g_n \cos\phi_n = z \cos(N - kr) + y_n' \sin(N - kr) \quad (n = i \text{ or } j). \quad (8)$$

To eliminate y_n' and g_n appearing in Eqs. (7) and

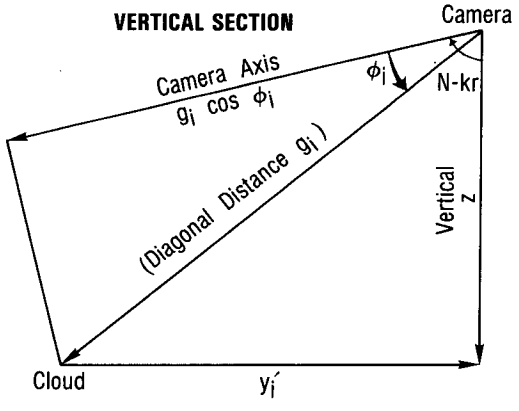

FIG. 4. A vertical plane through the camera axis. Resolved along the direction of the camera axis, the diagonal distance g_i is of length $g_i \cos\phi_i$ in this plane. The horizontal distance y_i' appears in Fig. 3. It is measured on a plane normal to the vertical through the camera. The camera is at a height z above this plane.

(8), note that g_n^2 is equal to

$$\sec^2\phi_n[z\cos(N-kr)+(y_n\cos\lambda_n+x_n\sin\lambda_n)\times\sin(N-kr)]^2=x_n^2+y_n^2+z^2 \quad (n=i \text{ or } j). \tag{9}$$

In this equation, ϕ_n, $(N-kr)$ and λ_n are measured angles. Aiming at relationships between x_i and y_i, and x_j and y_j, first an expression for z is obtained: From Fig. 5

$$z \sim \bar{y}\cot\gamma, \tag{10}$$

where the nadir angle γ of the cloud is given by

$$\gamma=(N-kr)+\tan^{-1}(e/F) \tag{11}$$

After substituting Eq. (10) into (9), it is found that terms in $\bar{y}$ are all much smaller than terms in y_n. With $\bar{y} \sim y_n$ [Eqs. (4) and (5)], $\bar{y}$ may be replaced by y_n. Then Eq. (9) is divided all through by y_n^2, and a quadratic equation results for the ratio $x_n/y_n = x_{1n}$.

$$x_{1n}=[B\pm(B^2-AC)^{0.5}]/A, \tag{12}$$

where

$$A=1-\sec^2\phi_n\sin^2\lambda_n\sin^2(N-kr),$$

$$B=\sec^2\phi_n\sin\lambda_n\sin(N-kr)\times[\cot\gamma\cos(N-kr)+\cos\lambda_n\sin(N-kr)],$$

$$C=1+\cot^2\gamma-\sec^2\phi_n\times[\cot\gamma\cos(N-kr)+\cos\lambda_n\sin(N-kr)]^2.$$

In Eq. (12), the positive (negative) square root is taken if the sign of $(d-d_n)$ in Fig. 1 is positive (negative). From Eqs. (4) and (5), the ratio

$$x_{1i}=x_i/[\bar{y}-0.5kv_ct\sin(c-\theta)] \tag{13}$$

and

$$x_{1j}=x_j/[\bar{y}+0.5kv_ct\sin(c-\theta)]. \tag{14}$$

The mean range $\bar{y}$ now may be obtained by substituting Eqs. (13) and (14) into (2), eliminating x_i and x_j.

$$\bar{y}=[x+0.5v_ct\sin(c-\theta)(x_{1i}+x_{1j})+v_ct\cos(c-\theta)]/k(x_{1i}-x_{1j}). \tag{15}$$

Where v_a is the speed of the aircraft, the distance x between frames n_i and n_j is v_at. Where s is the interval between movie frames,

$$t=s(n_j-n_i) \tag{16}$$

so

$$x=v_as(n_j-n_i). \tag{17}$$

With the range of the cloud $\bar{y}$ obtained from Eqs. (15) to (17) the problem is essentially solved.

The frame number n_x at which the aircraft is nearest to the cloud is obtained after referring to Fig. 2

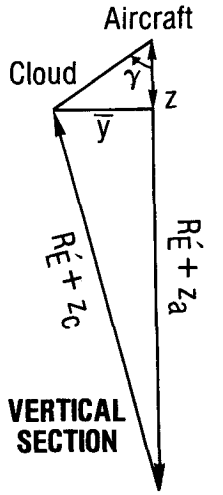

FIG. 5. Vertical plane through aircraft and cloud at frame n_m (see Fig. 1). Verticals through the aircraft and the cloud meet at the center of the earth, of radius R_E. (To compensate for refraction, $R'_E = 1.25R_E$ is used instead of R_E). The heights z_a and z_c are those of the aircraft and cloud, respectively, above the surface. At frame n_m, the nadir angle of the cloud is γ.

and Eq. (13):

$$n_x \approx n_i+\{x_{1i}[k\bar{y}-0.5v_ct\sin(c-\theta)]-0.5v_ct\cos(c-\theta)\}/(v_as). \tag{18}$$

Usually $n_x \sim n_m$. Sometimes $n_x \neq n_m$, when the cloud becomes obscured before it reaches the middle of the field of view. Then the elevation measurement e (Fig. 1) has to be referred to a point relatively remote from the principal point of the camera—with some (slight) loss of accuracy.

The height z_c of the cloud above the surface is obtained after using the sine formula on the triangle outlining Fig. 5:

$$z_c \approx z_a-\bar{y}\cot\gamma+0.5\bar{y}^2/R'_E. \tag{19}$$

Here R'_E is the local radius of curvature of the earth (~6360 km) multiplied by 1.25 to compensate for refraction [see Battan (1973, p. 24) for the rationale and Born (1966, p. 396) for refractive index formulas]. The last term in Eq. (19) commonly contributes 100 m, more for a cloud at great range $\bar{y}$.

The width of the cloud w is obtained from its width w_m measured on the projection screen at frame n_m (Fig. 1). As may be seen using Fig. 5

$$w \sim \bar{y}\,\mathrm{cosec}\gamma(w_m/F) \tag{20}$$

for small w_m. This completes the formulation of the problem.

4. Test measurements and discussion

The measurements described here began with a study of Great Natuna Island in the South China

TABLE 1. Results for various points called *A* to *D* on Great Natuna Island (each line refers to an independent measurement).

Point	Errors Δz_c (km)	Errors Δy (km)	Errors Δx (km)	Range $\bar{y}$ (km)
A	0.01	−1.3	0.5	21.7
A	0.09	−1.5	0.4	21.5
B	−0.11	−1.6	0	30.3
C	0.08	−1.5	−0.4	42.6
D	−0.05	1.3	0	43.8
D	−0.12	1.3	0	43.8
D	−0.02	1.3	0	43.8
D	0.01	1.3	0	43.8
D	0.01	1.3	0	43.8
D	0.04	1.0		43.2
D	−0.02	1.0		43.2
D	0.08	1.0		43.2
D	0.10	1.0		43.2
D	0.11	1.0		43.2

Sea, viewed from the WP3D aircraft. Four points on the coastline were measured, at various ranges from the aircraft. The horizontal locations of these points were known to about ±2 km. Their heights z_c were known to be zero. Tests were made for various combinations of the fixed parameters F (the effective focal length), N (the nadir angle of the camera) and ψ (the amount by which the camera was pointed behind the normal to the aircraft heading). The chosen values $F = 10.2$ mm (multiplied by the magnification), as opposed to the nominal value 10 mm for the camera, $N = 88.2°$ and $\psi = 0.2°$ yielded the results shown in Table 1. Of chief concern are the height errors Δz_c. These are within 120 m of zero, even for points more than 40 km from the aircraft and 7 km below it—results very difficult to better. The sensitivity of height to N is $\sim$100 m $(0.2°)^{-1}$ at range 30 km; the sensitivity to F is about 20 m $(0.3 \text{ mm})^{-1}$, which is small. Thus N—and elevation measurements—must be correct to a few tenths of 1° for accuracies in height of a few hundred meters. An error in focal length of 0.1 mm is unimportant. The sensitivity of range $\bar{y}$ to focal length is 0.9 km $(0.3 \text{ mm})^{-1}$ at range 30 km. The angle ψ should be correct to a few tenths of 1°.

Practical experience has shown that for accurate height measurements great care is required in measurement of elevation, in particular the coupling of the measurement e in Fig. 1 with an accurate elevation datum. This may be either the visible horizon, or as described here the roll of the aircraft at the frame of measurement of e. The chief source of random height uncertainty in MONEX work has been the matching of movie frame number n to the roll r. The movies taken from the WP3D on 10–12 December involved irregularities of frame interval—irregular camera operation—which required close study. Between turns the roll was quite steady, so inaccuracies are not too great. The Electra movies were good—but with oscillation the roll changed continuously, so that accurate timing was important. To minimize this problem, e was measured at times of small dr/dt.

The next most important precaution in the measurement process is the inclusion of a rough value of cloud velocity, where this is great, as described in Section 2. Failure to account for a cloud motion of 15 m s^{-1} may be likened roughly to a 5% error in focal length (F); it would typically lead to a height error of 500 m.

Inclusion of the difference between the track and the heading of the aircraft (and of the small angle ψ) in WMONEX commonly leads to improvement in height estimates of 100 m or less. It is worthwhile for cases involving slight turns in the track (as with an oscillation); worthwhile if good estimates of horizontal positions of distant clouds are wanted, and would be important for flight at large drift angles (large values of λ in Fig. 3), across the direction of strong winds, as in a hurricane.

5. Categories of cumulus clouds

Cumulus clouds in the size ranges fractus, humilis, mediocris, congestus and cumulonimbus are generally recognized (WMO, 1969). Fractus and humilis are illustrated in Fig. 6, mediocris, congestus and cumulonimbus in Fig. 7. For 10 December 1978 over the South China Sea, measurements of depth and width of updraft of cumulus fractus and humilis clouds are shown in Figs. 8a and 8b, and of height and width of mediocris, and congestus and cumulonimbus, in Figs. 8c and 8d. Often the clouds con-

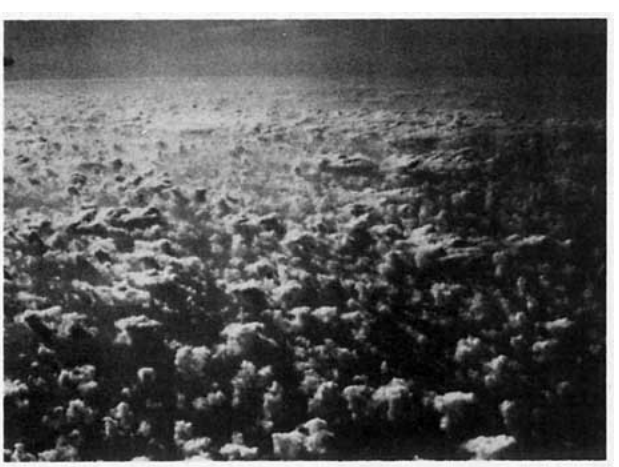

FIG. 6. 10 December 1978, 0736 GMT. Photograph by Charles Warner looking westward from the WP3D flying at altitude 7.8 km at 14.7°N 116°E. Fractus and humilis with great number density were distributing moisture and heat from the surface upward to altitude $\sim$1.3 km, through a cold northeasterly monsoon flow constrained beneath a stable layer. These clouds are represented by the integers 13 in Figs. 8a and 8b.

sisted of prominent towers rising out of a larger mass. [Warner *et al.* (1973) described how cumulus towers grow as a succession of elements appearing through a rising summit.] In the diagrams for the larger clouds, some pairs of width measurements are shown, joined by horizontal lines, to illustrate this phenomenon.

For cumulus fractus, a depth of 0.2 km and width of 0.25 km was typical; for humilis, 0.7 and 0.4 km. These clouds were based near 500 m. The spectrum of cloud sizes was seen to be continuous through the two categories, which were very probably closely related to transfer of heat and moisture upward through the predominantly unstable lowest kilometer of the northeasterly monsoon flow. Distinction between fractus and humilis here represents a crude attempt to describe a continuous spectrum in terms of two halves.

Mediocris clouds occurred with much lesser number densities than fractus and humilis. Heights were near 2.2 km, and widths near 1.3 km. These clouds commonly spread out at the level of a stable layer capping the monsoon flow.

Congestus clouds generally were isolated, relatively slender towers. In Fig. 8d, a representative line has been drawn by eye, to describe approximately the increase in width (w) of rising thermals with height (z). With units in meters

$$w \approx 550 + 0.17(z - 500).$$

For day 245 of the GARP Atlantic Tropical Experiment, Warner (1980) obtained by similar methods the equation

$$w \approx 300 + 0.26(z - 500).$$

The clouds, and these two equations, are sufficiently similar to hold promise for the development of a general model for individual tall cumulus towers over tropical oceans.

6. Measurement of cloud number density and fractional area coverage

This is based on the ability to recognize by eye clouds in the categories described above, and on counting their numbers in a known area of a projected image. The chief difficulties of measurement are in recognizing the existence of small fractus, in distinguishing between a large fractus and a small humilis, and in assigning representative widths to the cloud categories in order to obtain fractional area coverage.

A suitably sized rectangular card of vertical dimension p and horizontal dimension $2q$ was placed symmetrically on the projected image of the cloud field of interest, and the number u of clouds appearing within its borders was counted (see Fig. 9a). The elevation $-e_t$ of the top edge of the card was

FIG. 7. 10 December 1978, 0838 GMT. Photograph by R. H. Simpson looking toward 220° from the WP3D flying at altitude 7.8 km at 9.2°N 114.7°E. Congestus clouds occurred to the north of a dark mass of cumulonimbus 300 km distant, which was later penetrated. The clouds are similar to those represented by the integers 16 and 17 in Fig. 8.

measured, and the roll angle r of the aircraft was noted for the movie frame projected. The cloud height corresponding to the count was assessed; often it was about two thirds of the way up through the depth of a typical cloud. This height z_u and a typical cloud width w were written down, based on measurements as described above. The width w corresponds with the width of updrafts, rather than encompassing irregular inactive cloud matter. The fractional area coverage by updrafts was about an order of magnitude less than that of inactive cloud debris (which intercepts radiation). The other input data were the focal length F and the height of the aircraft z_a.

The rectangular card on the projection screen delineated an area in plan at height z_u which was bounded by lines of roughly constant azimuth (the vertical edges) and range (the horizontal edges), as shown in Fig. 9b. It was nearly a triangle with its apex at the aircraft position—truncated by the lower horizontal edge at close range—and with a wide base at great range defined by the upper edge.

An arbitrary point on a vertical edge of the card has a horizontal location x, y as shown in Fig. 9b. Referring to Eq. (9) it is appropriate to set $\lambda_n = 0$, and to replace x_n, y_n, ϕ_n by x, y, ϕ and z by $z_a - z_u$:

$$\sec^2\phi[(z_a - z_u)\cos(N - kr) + y\sin(N - kr)]^2 = x^2 + y^2 + (z_a - z_u)^2. \quad (21)$$

Eq. (10) in this context becomes

$$z_a - z_u \sim y\cot\gamma \quad (22)$$

with γ as in Eq. (11). Here the elevation measure-

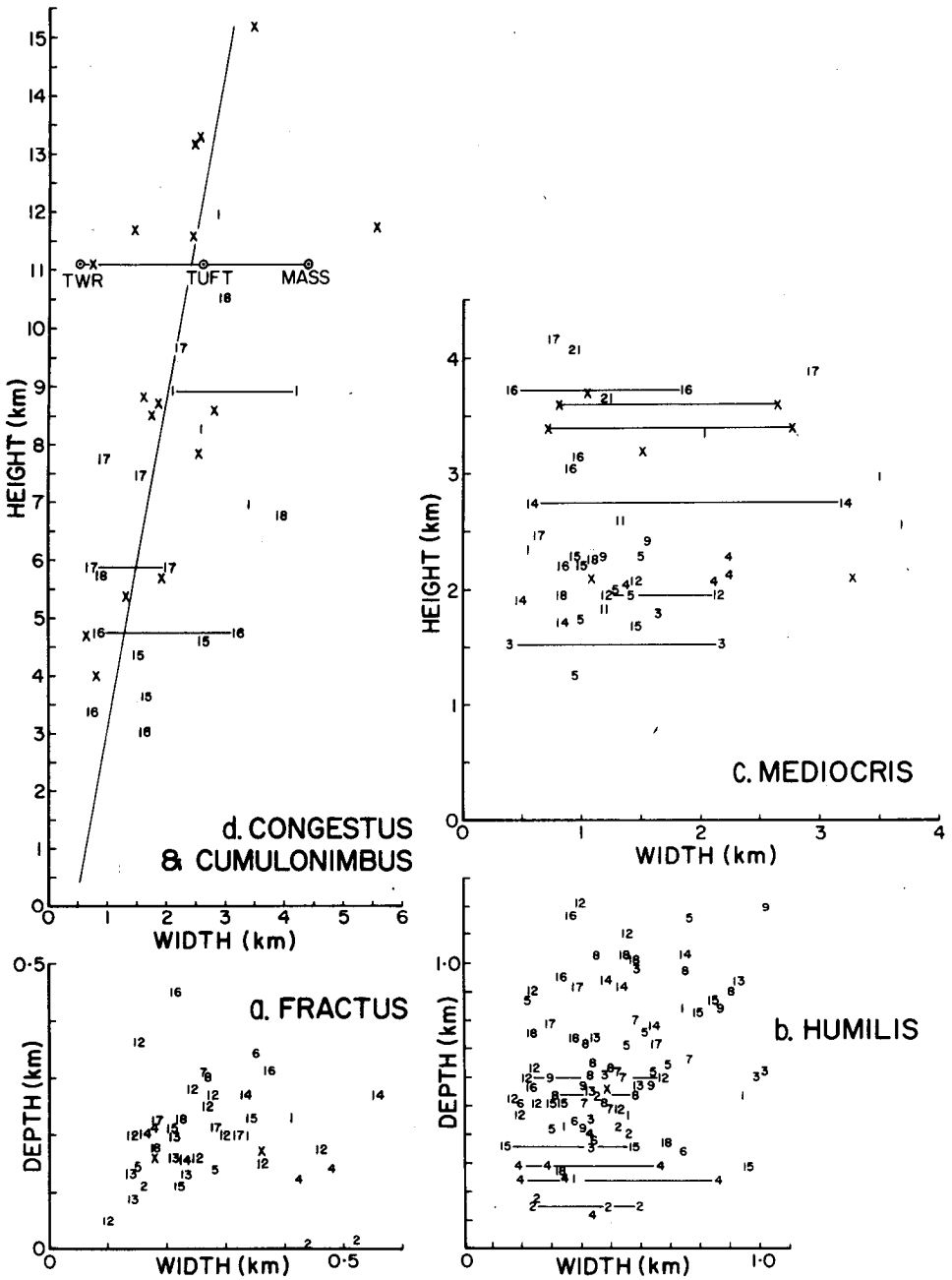

FIG. 8. 10 December 1978. Depth or height above the sea of cumulus clouds as a function of width of updraft, in the size categories *a*, fractus; *b*, humilis; *c*, mediocris, and *d*, congestus and cumulonimbus. Most measurement points are shown as small integers (1–21) referring to proximity to a corresponding dropwindsonde released from the WP3D aircraft. Pairs of measurements joined by horizontal lines show the widths of both small rising towers and the cloud masses from which the towers emerged. In *d*, a line has been drawn by eye to describe approximately the increase of width of updrafts with height.

ment e lies in the range $-e_t$ to $-e_t - p$. Following Eq. (1), the angle ϕ is given by

$$F^2 \tan^2\phi = q^2 + e^2. \tag{23}$$

By substitution into Eq. (21), it is found that

$$x = qy/[F \sin(N - kr) + e \cos(N - kr)]. \tag{24}$$

The plan view area A outlined by the rectangular card is given by

$$A = \int_{y_1}^{y_2} 2x dy, \tag{25}$$

where y_2 and y_1 represent the extremes of range cor-

responding to the upper and lower horizontal edges of the card. From Eq. (22),

$$y_2 = (z_a - z_u) \times \tan\{(N - kr) - \tan^{-1}[e_t/F]\}, \quad (26)$$

$$y_1 = (z_a - z_u) \times \tan\{(N - kr) - \tan^{-1}[(e_t + p)/F]\}. \quad (27)$$

Performing the integration in Eq. (25) yields

$$A = [(y_2 + y_1)\sin(N - kr) + 2(z_a - z_u) \times \cos(N - kr)](y_2 - y_1)q/F. \quad (28)$$

This area is divided by the number of clouds u to obtain the inverse cloud number density or area per cloud. The fractional area coverage by cloud is given by

$$\sigma = 0.25\pi w^2 u/A. \quad (29)$$

Uncertainties in u are substantial, as previously stated. Uncertainties in assignation of a value of w representative of many clouds is greater—and σ depends on w^2. Thus σ is only an order of magnitude estimate.

The size of the card ($p \times 2q$) is chosen to suit the clouds being counted. A small card is generally used for fractus and humilis, a larger one for mediocris. The whole screen may be used for mediocris and congestus. The top elevation e_t must not be too close to zero, because then the area A becomes very sensitive to e_t and to the roll r. A substantial value is usually used for e_t. With congestus sometimes visible out to great range, sometimes the outer range y_2 is estimated by eye rather than calculated using e_t. Some uncertainty arises from the assignation of z_u; this is less than that involved in the count of u.

Beyond these problems in obtaining cloud number density and fractional area coverage, there was mesoscale variability on a length scale of 100 km encompassing several orders of magnitude, as will be shown below.

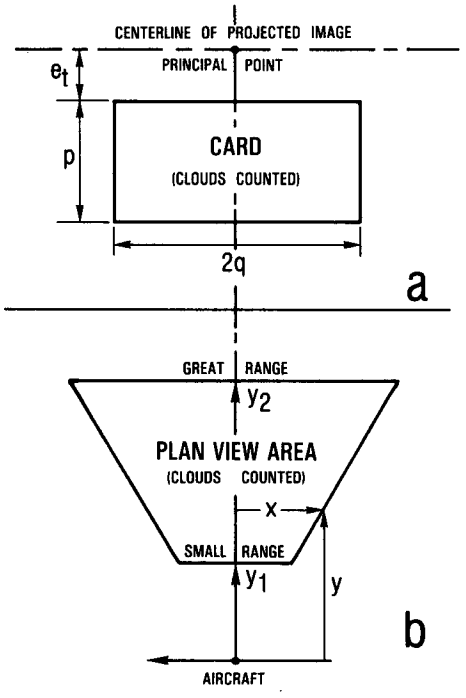

FIG. 9. (a) Projection screen with card for counting clouds placed symmetrically on it. (b) Plan view area covered by card.

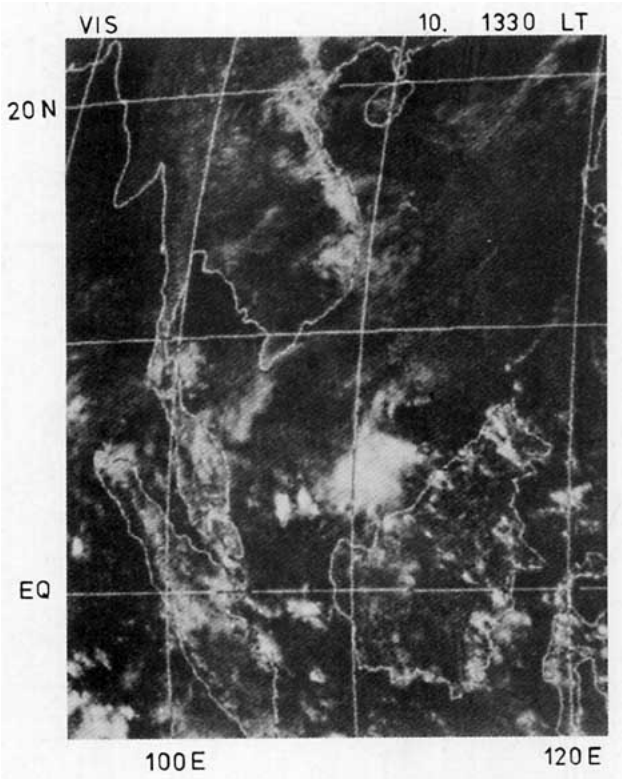

FIG. 10. 10 December 1978, 0533 GMT. Visible image of the South China Sea area from the satellite GMS-1 (from Sadler, 1979).

7. A cloud map for 10 December 1978

On this day, the WP3D flew from Kuala Lumpur to latitude 19°N and back, over the South China Sea, while the Electra flew a smaller circuit to 12.5°N within that of the WP3D. A visible image from the satellite GMS-1 is shown in Fig. 10 (reproduced from Sadler, 1979). A plan view map of the peak heights reached by cumulus towers originating near the surface is shown in Fig. 11. Each integer is a height (km) above the sea and applies to a square of 1° × 1°. Shading is used to draw attention to both suppressed and active areas. D means deep cumulonimbus. A few good measurements yield tops of width ~3 km reaching 15 ± 1.5 km. Brack-

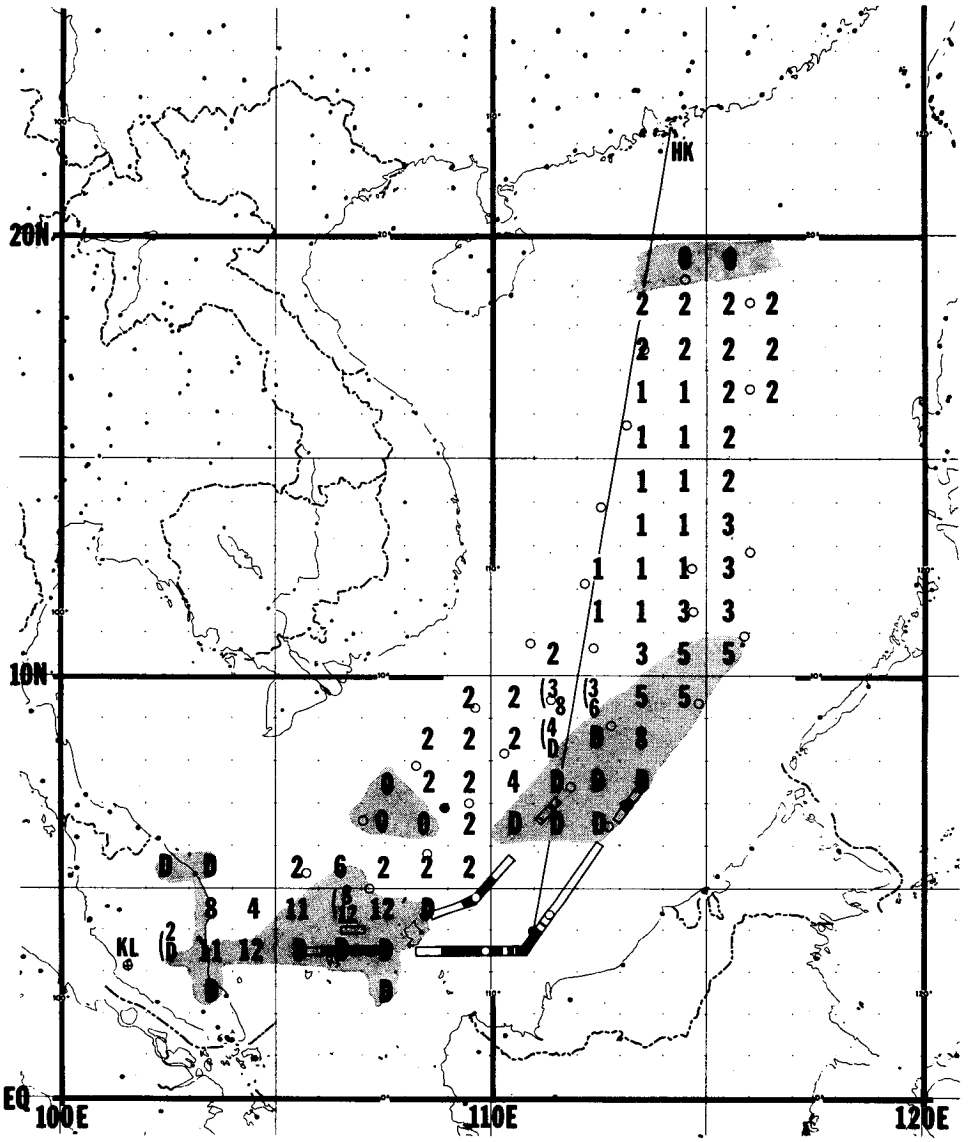

FIG. 11. 10 December 1978, 0230–1200 GMT. Peak heights (km) of cumulus towers originating near the surface, in 1° × 1° squares, as seen from the aircraft. Shading emphasizes deep clouds, and suppressed areas. KL = Kuala Lumpur. HK = Hong Kong. See text for further details.

eted pairs of values yield tops of earlier and later measurements, during the period of flight (0230 to 1200 GMT). Open boxing shows the track of the aircraft when flying below the dense high overcast clearly visible in Fig. 10, which extended down from anvil top level, about 12.5 ± 0.5 km, to about 9 ± 1 km. Solid boxing shows flight in cloud at 6.8 km (top, Electra) and 7.8 km (bottom, WP3D). Small circles show dropwindsonde locations. Solid small circles represent a triangle of Soviet ships.

Near 20°N there was a suppressed area (accompanied by strong subsidence). Between 19 and 17°N were many cumulus mediocris (just penetrating stratus at 1.9 km). Cloud streets along direction ~030°, with spacing ~2.5 km, prevailed from 17 to 11°N, and around to the north of an area of high cloud over the southern half of the Soviet ship triangle. This high cloud has been treated in the pair of papers by Houze *et al.* (1981) and Johnson and Priegnitz (1981). A clear area was present around 7°N, 108°E, followed by more streets in to the east Malaysian coast. Along the coast were congestus and cumulonimbus.

A separate discussion is planned of the several different regimes of weather revealed in the cloud map.

TABLE 2. 10 December 1978. Areas per cloud (A) and fractional area coverages by updrafts (σ) in different size categories.

Position			Fractus ~0.7 km (930 mb)		Humilis ~1.0 km (900 mb)		Mediocris ~1.8 km (820 mb)		Congestus ~3 km (710 mb)	
°N	°E	D/S**	A (km^2)	σ (%)	A (km^2)	σ (%)	A (km^2)	σ (%)	A (km^2)	σ (%)
17.5	113.8	Q 9					300	0.4		
17.4	113.7	Q 9	3.7	0.2	30	0.7				
					(3.4	3.5)				
16.7	115.7	Q 12	1.1	3	4.4	1.1	60	2.4		
16.6	113.5		Great	Small	12	1				
15.7	113.3	Q 8	1.2	2.7	15	1.4				
14.8	115.7		0.9	3.4	3.0	6.4				
13.7	112.7	Q 7	2.2	1.4	18	1.1				
12.9	115.7	Q 14	2.7	1.1	>2.8	<7	1000	0.1		
12.1	112.3	Q 6	2.1	1.5	16	0.8				
12,	115.7				8*	2.5	300	1.5		
11.8	112.2		1.1	2.8	5	2.5				
11,	115.7	Q 15	2	1.5	5.7	1.2	75	1.2	1000	0.3
10.4	111.1	Q 5	~2	~1.5	3.7	5.5	25	4		
9.6	114.6	Q 16	4	1.2	10	0.7	100	0.8	550	0.3
9.6	114.4								200	0.8
9.1	109.8	Q 4	1.5	3.3	35	0.2	500	0.7		
7.7	113.3	Q 17	1.3	4	17	0.8	340	0.2	670	0.1
7.5	108.5	Q 3			Great	Small	200	0.9		
6.4	107.2	Q 2	1.2	4	7	3				
6.4	112.1		1.0	3	3.8	5	510	0.15		
3.8	104.4				2	6	100	3		
3.6	105.5		1.0	3	3.2	4				

* Locally.
** D/S are dropwindsondes (Q2, Q3, Q4 . . .) released sequentially.

8. Cloud population statistics

Inverse cloud number densities, or areas A per cloud, are shown with corresponding fractional area coverages by updrafts (σ, %) in Table 2, from the right side camera of the WP3D. Measurements were made at times of dropwindsonde release. Areas over which the counts were made were about 40, 100, 1000 and 2000 km^2 for fractus, humilis, mediocris and congestus, respectively. From continuous viewing of the films, cloud number densities were seen to vary over an order of magnitude within distances of 100 km.

Due to numerous coral reefs in the South China Sea, local variations of sea surface temperature are likely. Due to small drifting patches of stratus, local variations in radiation are likely. Therefore the mesoscale variability of cloudiness is not surprising.

In respect of cumulonimbus cloud number densities, nine cumulonimbi were counted at 0740 GMT in the 1° × 2° area bounded by 6 and 7°N and 100 and 112°E (25 000 km^2). If each cloud contained an updraft of width 2 km in the middle troposphere, $\sigma \approx 0.1\%$, a figure similar to those for congestus in Table 2. If the mean updraft was 5 m s^{-1} in the clouds and zero everywhere else, the clouds were equivalent to an area mean lifting of ~ -1.5 mb h^{-1}. If this lifting was continuous from near the surface, and originated solely from uniform horizontal convergence throughout the lowest 500 m of the 1° × 2° area, then this convergence was $\sim 8 \times 10^{-6}$ s^{-1}. This number appears to be relatively small. The presence of the deep clouds is seen to be due primarily to heating of the low-level monsoon flow during prolonged passage over the South China Sea, coupled with diminishing subsidence in the mid-troposphere southward from 17 to 10°N (not shown here).

9. Conclusions

A new method of photogrammetry of clouds from aircraft side camera movies has been described, which can cater for uniform motion of a cloud, the motion being deduced subjectively from the wind field determined independently. This method has led to better estimates of cloud heights, by up to 500 m in extreme circumstances of measurement. Typical improvements are on the order of 100 m. Use of the method is desirable when cloud measurements are related to other data.

A method of measuring cumulus cloud number densities has been developed also, in the size categories fractus, humilis, mediocris and congestus. Uncertainties of roughly a factor 2 accompany these measurements, chiefly due to problems of recognizing individual clouds. Extension to measurement of fractional area coverage by updrafts yields order of magnitude estimates.

Application of these techniques to clouds of 10 December 1978 over the South China Sea has resulted in findings as follows:

For cumulus fractus, a depth of 0.2 km and updraft width of 0.25 km were typical; for humilis, 0.7 and 0.4 km. These clouds together formed a continuous spectrum, with number density up to ~1.5 clouds km^{-2}, and with up to ~10% area coverage by updrafts. These numbers varied down to zero, even in circumstances relatively uniform on a scale of hundreds of kilometers.

Cumulus mediocris typically reached a height of 2.2 km or more, and their updrafts were of width ~1.3 km. Number densities, very variable, occasionally reached one per 25 km^2; area coverage by updrafts sometimes reached a few percent. Coverage by congestus was less than that by the smaller clouds. Nine cumulonimbi were counted in an area measuring 1° × 2°, yielding one cloud per 3000 km^2, and ≈0.1% coverage by updrafts in mid-troposphere.

Acknowledgments. I thank R. H. Simpson and B. J. Morrison for provision of synoptic data, and for helpful comments; Jim Hamm for drafting and Jackie Harding for typing. Careful reviews are greatly appreciated. This material is based upon work supported by the Division of Atmospheric Sciences, National Science Foundation, under Grants ATM-7900233 and ATM-8012214.

APPENDIX

Measuring Elevations from the Aircraft Time-Lapse Movies

Fig. 1 shows a centerline of the projected image drawn horizontally. For the WP3D aircraft, the center of this line was taken as the principal point, on the camera axis. In practice it is easiest to measure elevations e from the top or bottom of the projected image, and adjust them with a constant to the centerline. The distance e measured from an arbitrary point on the centerline remains equal to that measured from the principal point if the drift angle λ in Fig. 3 is zero. Unless the drift angle is great, it does not matter if the cloud is not precisely aligned in the vertical with the principal point when e is measured.

For the Electra aircraft, small fiducial arrowheads at left and right protrude into the movie images. If the roll of the aircraft is zero, these show the level of the horizontal. It was found that for each new film loaded into an Electra camera, images appeared in a new vertical position. With measurements e made from top or base of the images, different adjustment constants for each film were used in referring the measurements to the horizontal, using the small fiducial arrowheads which remained fixed.

REFERENCES

Battan, L. J., 1973: *Radar Observation of the Atmosphere.* University of Chicago Press, 324 pp.

Born, C. J., Ed., 1966: Mechanical methods of phototriangulation. In *Manual of Photogrammetry,* Third Edition, Amer. Soc. Photogramm, Falls Church, pp. 377–459.

Greenfield, R. S., and T. N. Krishnamurti, 1979: The Winter Monsoon Experiment—Report of December 1978 field phase. *Bull. Amer. Meteor. Soc.,* **60,** 439–444.

Houze, R. A., Jr., S. G. Geotis, F. D. Marks, Jr., and A. K. West, 1981: Winter monsoon convection in the vicinity of North Borneo. Part I: Structure and time variation of the clouds and precipitation. *Mon. Wea. Rev.,* **109,** 1595–1614.

Johnson, R. H., and D. L. Priegnitz, 1981: Winter monsoon convection in the vicinity of North Borneo. Part II: Effects on large-scale fields. *Mon. Wea. Rev.,* **109,** 1615–1638.

Malkus, J. S., 1952: The slopes of cumulus clouds in relation to external wind shear. *Quart. J. Roy. Meteor. Soc.,* **70,** 530–542.

Sadler, J. C., 1979: Synoptic scale quick look for winter MONEX—December 1978. Rep. UHMET 79-02, Dept. of Meteorology, University of Hawaii, Honolulu, 66 pp.

Telford, J. W., and P. B. Wagner, 1974: The measurement of horizontal air motion near clouds from aircraft. *J. Atmos. Sci.,* **31,** 2066–2080.

Warner, C., 1972: Calculations of updraft shapes in storms. *J Atmos. Sci.,* **29,** 1516–1519.

——, 1978: Photogrammetry from aircraft nose camera movies. *J. Appl. Meteor.,* **17,** 1416–1420.

——, 1980: Cloud Measurements on day 245 of GATE. *Atmos.-Ocean,* **18,** 207–226.

——, J. H. Renick, M. W. Balshaw and R. H. Douglas, 1973: Stereo-photogrammetry of cumulonimbus clouds. *Quart. J. Roy. Meteor. Soc.,* **99,** 105–115.

——, J. Simpson, D. W. Martin, D. Suchman, F. R. Mosher and R. F. Reinking, 1979: Shallow convection on day 261 of GATE: Mesoscale arcs. *Mon. Wea. Rev.,* **107,** 1617–1635.

WMO, 1969: *International Cloud Atlas.* WMO, 62 pp.